LA-UR- 07- 1607

Approved for public release; distribution is unlimited.

Title: ON PIEZOELECTRIC LAMB WAVE-BASED STRUCTURAL HEALTH MONITORING USING INSTANTANEOUS BASELINE MEASUREMENTS

Author(s): Steven R. Anton, LANL, WT-2
GyuHae (NMI) Park, LANL, INST-OFF
Charles R. Farrar, LANL, INST-OFF
Daniel J. Inman, Virginia Tech

Submitted to: SPIE INTERNATIONAL SYMPOSIUM ON SMART STRUCTURES AND NONDESTRUCTIVE EVALUATION,SAN DIEGO, CA, MAR. 18-22, 2007.

Los Alamos
NATIONAL LABORATORY

On piezoelectric Lamb wave-based structural health monitoring using instantaneous baseline measurements

Steven R. Anton[1], Gyuhae Park[2], Charles R. Farrar[2], Daniel J. Inman[1]

[1]Center for Intelligent Material Systems and Structures
Virginia Polytechnic Institute and State University, Blacksburg, VA 24060
[2]The Engineering Institute, Los Alamos National Laboratory, Los Alamos, NM 87545

ABSTRACT

A critical aspect of existing Structural Health Monitoring (SHM) systems is the ability to compare current data obtained from a structure to a prerecorded baseline measurement taken for an undamaged case. Several Lamb wave-based SHM techniques have been successfully developed that use baseline measurements to identify damage in structures. The method developed in this study aims to instantaneously obtain baseline measurements in order to eliminate any complications associated with archiving baseline data and with the effects of varying environmental conditions on the baseline data. The proposed technique accomplishes instantaneous baseline measurements by deploying an array of piezoelectric sensors/actuators used for Lamb wave propagation-based SHM such that data recorded for equidistant sensor-actuator path lengths can be used to instantaneously identify several common features of undamaged paths. Once identified, data from these undamaged paths can be used as a baseline for near real-time damage detection. This method is made possible by utilizing sensor diagnostics, a recently developed technique which minimizes false damage identification and measurement distortion caused by faulty sensors. Several aspects of the instantaneous baseline damage detection method are detailed in this paper including determination of the features best used to identify damage, development of signal processing algorithms used to analyze data, and a comparison of two sensor/actuator deployment schemes.

Keywords: structural health monitoring, instantaneous baseline, piezoelectric, lamb wave propagation

1. INTRODUCTION

In recent years, several successful impedance and Lamb wave-based Structural Health Monitoring (SHM) systems have been developed.[1-5] A key component of these systems is the comparison of newly recorded data to a baseline measurement taken from a healthy structure. The baseline data represents the dynamic signature of the structure when no damage is present. Differences between current data and baseline measurements are used as indications of damage in the structure. Although the success of these techniques has been proven, the measurement and storage of baseline data remains challenging. Varying temperature and environmental conditions can cause significant deviations in the data recorded from an undamaged structure that, when compared to baseline data, can falsely indicate damage. Relying on a pre-recorded baseline measurement for damage detection requires an appropriate data storage system to be implemented, and also implies that the damage detection system will be incapable of assessing the health of a structure if baseline data is lost or unavailable. Additionally, complications arise when attempting to implement an SHM system on a structure that has already been placed into service. Baseline measurements taken on aging structures will be insensitive to preexisting damage and insufficient for use in assessing the current condition of the structures. The current research works to alleviate some of the complications of current SHM methods by instantaneously acquiring a baseline measurement on a structure, thus eliminating the effects of varying environmental conditions and the need to store a pre-recorded baseline. Several technologies including piezoelectric actuation and sensing, Lamb wave propagation, and a method of assessing the condition of piezoelectric sensors referred to as 'piezoelectric active-sensor diagnostics,' will be combined to achieve this goal.

This study focuses on Lamb wave-based SHM using piezoelectric materials. The electromechanical coupling effect of piezoelectric material allows it to act as a sensor and an actuator, allowing Lamb waves to be both induced and measured

with the same device. The Lamb wave propagation technique used in SHM deploys an array of piezoelectric patches that act as both sensors and actuators onto a test structure. A single patch is used as an actuator to induce a mechanical wave in the structure while data is recorded from nearby piezoelectric sensors to capture the wave as it travels through the material. By allowing each patch to act as an actuator and recording the response from nearby patches, an array of patches can monitor an entire structure. Lamb waves are an attractive type of mechanical wave for SHM because they can propagate over long distances in thin plates, their velocity is predictable, they are sensitive to surface damage, and they are easily excitable with piezoelectric devices. A detailed explanation of Lamb wave theory is presented by Viktorov.[6]

The instantaneous baseline method developed in this study involves deploying an array of equally spaced Lead Zirconate Titanate (PZT) transducer patches on a 4 ft (1.22 m) square aluminum plate with uniform properties. The PZT transducers are used for pitch-catch Lamb wave propagation-based SHM. Signals are recorded and compared for equal length paths such that common features of undamaged paths can be identified, thus creating an instantaneous baseline. Assuming that signals from equal length, undamaged paths will exhibit consistent features, a damaged path can be separated from undamaged paths in near real-time by using data processing methods that look for changes of a path's shape, magnitude, or frequency as compared to the features of the instantaneous undamaged baseline.

2. PIEZOELECTRIC SENSOR DIAGNOSTICS

A key component to any successful piezoelectric SHM system is the ability to assess the condition of the sensors and actuators installed on the structure being monitored. A technique referred to as 'piezoelectric active-sensor diagnostics' presents the ability to evaluate both the bonding condition between a piezoelectric transducer and its host structure, as well as the mechanical and electrical properties of the device.[7-8] Sensor/actuator malfunction is a major source of failure in SHM systems. Sensor/actuator fracture is the most common type of transducer failure, which can be attributed to the brittle nature of many piezoelectric devices. Additionally, maintaining sufficient bonding conditions between the transducer and host structure over the long service life of many SHM systems can be difficult. Changes in bonding condition or degradation of the mechanical/electrical properties of the transducer could cause false damage identification, compromising the ability of the SHM system to accurately evaluate the condition of the host structure.

The sensor diagnostics technique has been shown to successfully detect sensor/actuator faults by measuring the admittance of a bonded piezoelectric patch at various frequencies and comparing a plot of the imaginary part of the admittance versus frequency against plots from several bonded patches and a free patch.[7] Figure 1 shows admittance measurements from a free patch and from nine PZT patches bonded to an aluminum plate.

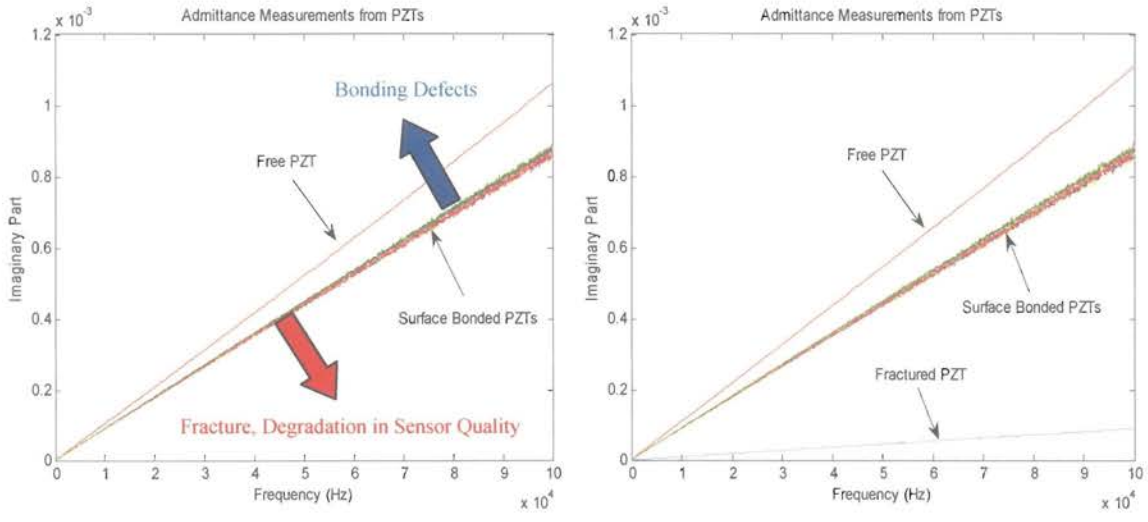

(a) Undamaged patches (b) Fractured patch

Figure 1: Electrical admittance measurements of surface bonded and free PZT patches

Physically, the slopes of the imaginary part of the admittance vs. frequency curves shown in Figure 1 represent the capacitive value of the piezoelectric devices. The capacitance of a patch changes with varying bonding condition or physical condition, therefore, the slope of the curve can be used to indicate the condition of a patch. Shown by the large arrows in Figure 1a, patches with an increased slope indicate a poor bonding condition; the extreme of which is the patch measured in the free condition. Patches with a decreased slope indicate a broken or otherwise degraded piezoelectric device. A detailed explanation of the sensor diagnostic technique used and the mathematical derivations supporting it can be found in the references.[7-8]

Figure 1a shows typical admittance measurements from several surface bonded PZT patches as well as a free PZT patch. From the figure it can be seen that the slope of all of the surface bonded patches is fairly uniform and the free patch has a considerably larger slope, which is in agreement with predicted results. Again, the figure also shows the potential effects of bonding defects and fracture or degradation of sensor quality. To confirm these results, one of the patches was fractured and the admittance of all the patches was measured again. Figure 1b shows a plot of the second data set. From the figure it is obvious that fracturing a patch caused its slope to decrease significantly, making the damaged patch easily identified.

The ability to diagnose the condition of PZT patches is critical to the success of the instantaneous baseline method developed in this study. The method relies on the fact that the shape, amplitude, and frequency of Lamb waves recorded for undamaged paths are same and that an instantaneous baseline can be created from undamaged measurements. If the patch that was identified as fractured in Figure 1b, for example, was used in this study, it is likely that there would be a false detection of damage in the plate. A poorly bonded or fractured patch would not transmit or receive the same amount of energy or consistency of signal as a well bonded, flawless patch, therefore, a faulty patch would be mistaken for damage in the structure.

3. EXPERIMENTAL SETUP AND PROCEDURE

A 4 ft (1.22 m) square, 0.0625 in (1.5875 mm) thick 6061-T6 aluminum plate was selected as the test specimen used in this study. The health of three aluminum plates was monitored using two piezoelectric configurations. Two aluminum plates were instrumented with an array of nine, 0.25 in (6.35 mm) piezoelectric devices that were super glued to the plate in a square pattern with 1 ft (0.30 m) between each patch. The deployment scheme of the first configuration can be seen in Figure 2a. A third aluminum plate was instrumented with thirteen patches fixed to the plate in a circular pattern with a radius of 18 in (0.45 m), as seen in Figure 2b. Two configurations were used to determine what role the sensor pattern had in the ability of the instantaneous baseline technique to detect damage.

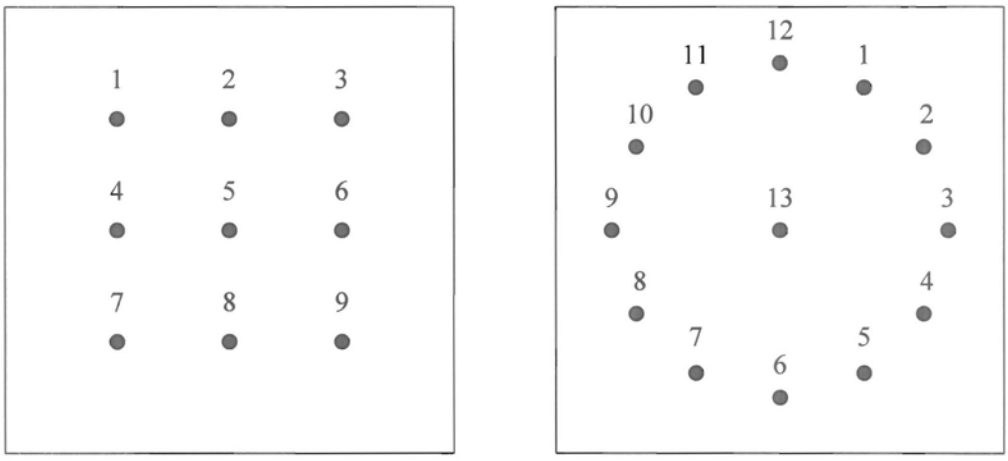

(a) Square configuration (b) Circular configuration

Figure 2: Piezoelectric sensor/actuator deployment schemes used for testing

In the test specimens described above, voltage data sets were taken for various path lengths for each configuration. Figure 3a shows the three different paths used in the square configuration. The total part coverage for the square pattern is shown in Figure 3b. Six different path lengths were used with the circular configuration. These path lengths along with the total part coverage can be seen in Figures 4a and 4b, respectively. Path lengths from patch 1 to 3 and 1 to 9 for the square pattern and path lengths from patch 12 to 6 for the circular pattern were not used because of redundancy.

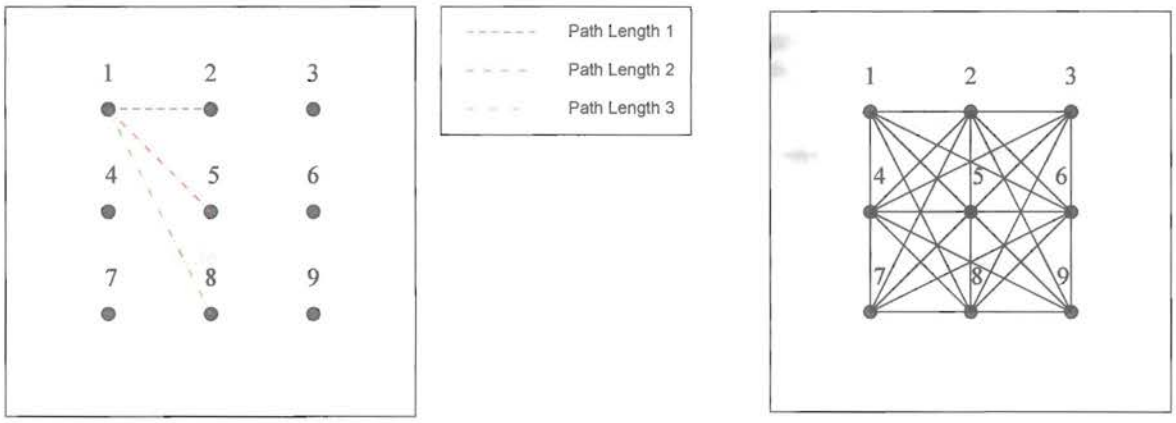

(a) Path lengths

(b) Overall part coverage

Figure 3: Various path lengths used and total part coverage for square configuration

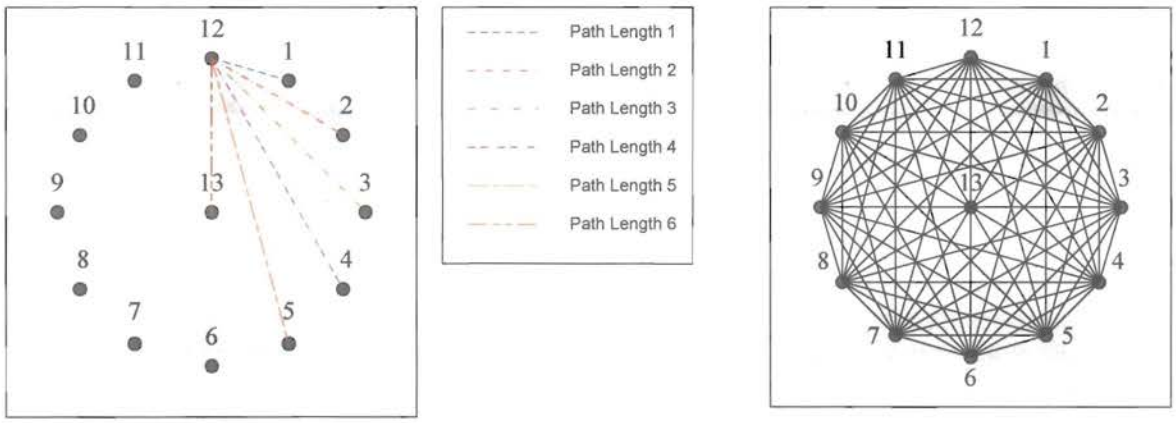

(a) Path lengths

(b) Overall part coverage

Figure 4: Various path lengths used and total part coverage for circular configuration

All of the data sets recorded were collected using a pitch-catch technique between the piezoelectric patches, through which each piezoelectric device acts as both a sensor and an actuator creating the paths seen in Figure 5. For example, a voltage signal would be passed through patch 1 of the square configuration which would strain the patch and excite a Lamb wave in the plate. Patch 2 would then be used as a sensor to measure the strain caused by the Lamb wave at that location. This strain is converted into a voltage by the piezoelectric patch, which is then recorded by the data acquisition system. A 5 V, 60 kHz burst sinusoidal waveform was used to excite the piezoelectric actuators. The voltage and excitation frequency were chosen after several experiments were run to determine the parameters that gave the cleanest, most consistent signal that could best be used to detect damage. It should be noted that the 5 V signal generated by the data acquisition program is sent through an amplifier. The final voltage to each PZT patch is approximately 15 V. When analyzing excitation frequencies, a trade-off between low frequencies and high frequencies was encountered. Signals with lower excitation frequencies have larger wavelengths and reduced the systems' overall sensitivity to

detecting damage, making higher frequency signals desirable. Lower frequencies, however, help maintain speeds of the A_0 and S_0 modes that result in little to no interaction between the first arrivals of the two modes at each sensor. It was also found that higher frequency signals gave more variation in signals from undamaged paths. A frequency of 60 kHz was found to be large enough to be sensitive to damage, but small enough to result in little mode interaction and variation in undamaged paths. Upon analyzing the effects of damage on both the A_0 and S_0 modes, it was determined that the A_0 is more sensitive to surface damage and will be analyzed in this study.

4. DATA PROCESSING TECHNIQUES

Three data analysis methods were developed to analyze the Lamb wave response data collected from each aluminum plate. Each method is applied to the first A_0 mode wave arrival for all paths of equal length. The first technique is based on the calculation of cross correlation coefficients for signals acquired over equal length paths to see how well the signals correlate. The second method involves calculating the area under the power spectral density curve for each signal to monitor the energy transferred across each path. The third technique is based on the proper orthogonal decomposition of each signal to investigate the dominant vibration modes present in the signals. The statistical nature of these analysis techniques requires that there be a reasonably large ratio of undamaged to damaged paths. This condition is especially true in the case of multiple damaged paths, which will skew the statistical methods with which the instantaneous baseline measurements are created if enough undamaged paths are not present. A detailed description of each data processing technique is described below.

4.1 Detailed description of cross correlation analysis technique

The first technique developed involves the cross correlation analysis of each signal compared to signals of the other paths of equal length. Cross correlation analysis determines the degree to which two signals are linearly related. Using this method, paths with outlying characteristics can be recognized when compared to other paths of equal length. In order to determine damaged paths, the modified cross correlation value is determined for each path. This technique involves first calculating the cross correlation values of a single reference path compared to all the other paths. Each comparison calculation yields one value. The function used to compute the cross correlation value allows for a phase shift to account for small differences in plate characteristics and sensor placement. Several cross correlation values are calculated by shifting one of the signals both positively and negatively, and the peak value is found. The peak values for each path combination are then subtracted from one and then that decimal is squared, causing outlying paths to have a significantly higher value than that of a statistically common path. All of these squared values are then summed and the process is repeated using each path as a reference. This process is shown mathematically in (1) where i represents the reference path index, j represents the various path combinations, and a is the peak cross correlation value for each path combination.

$$e(i) = \sum_{j=1}^{n} \left(1 - |a(j)|\right)^2 \tag{1}$$

The purpose of the cross correlation method is to detect damaged paths by investigating the effects of removing a potentially damaged path from the data set and recalculating the cross correlation values. If a damaged paths exists in the data set, then the cross correlation values calculated when the damaged path is compared to all of the other paths will be significantly higher than values comparing undamaged paths. If the damaged path is removed from the data set, then the sum shown in (1) will decrease for every remaining path because sum will no longer include the correlation value calculated by comparing the paths to the damaged path. Based on this fact, the cross correlation technique works by calculating the percent difference between the sum of the original values of e in (1) when the damaged path was included in the calculations and the sum of the new values of e after the damaged path is removed from the data set. To calculate this percent difference, the path with the worst correlation, i.e. greatest value of e in (1), is removed from the data set and the cross correlation procedure is performed again on the remaining paths. This is shown mathematically in (2), where b is the new sum. These new cross correlation coefficients need to be scaled after performing the summing operation shown in (2). Scaling is necessary for comparison purposes because the sum shown in (2) represent the addition of only the remaining paths (one less than the original values calculated). Because each value of b represents

the sum of one less number than the values of e, the new b values are scaled up by adding the average of b back into b according to (3). The scaled values are shown as c in (3).

$$b(i) = \sum_{j=1}^{n-1} \left(1 - |a(j)|\right)^2 \tag{2}$$

$$c(i) = b(i) + \frac{b(i)}{n-1} \tag{3}$$

The new correlation values, c, are then summed together, shown in (4). The correlation values of all paths from the original cross correlation performed are also summed and the magnitude of the least correlated path, shown as path g, is subtracted. This process is shown in (5).

$$d = \sum_{i=1}^{n-1} c(i) \tag{4}$$

$$f = \left(\sum_{j=1}^{n} e(i) \right) - e(g) \tag{5}$$

The percent difference between these two numbers is then calculated, shown mathematically in (6), to determine how much the removed path affected the cross correlation values of the remaining paths. This path removal technique is repeated as many times as necessary until a relatively small percent difference is reached. When the desired percent difference is reached, the paths that were previously removed can be designated as damaged.

$$percent \quad difference = \left(\frac{f-d}{f} \right) * 100 \tag{6}$$

Using this technique it is necessary to set a threshold on the percent differences to detect damage, but not a threshold for the actual cross correlation values calculated. As long as a typical percent difference for an undamaged structure can be estimated, this cross correlation method can detect damage without the use of a pre-recorded baseline data set. Typical percent differences of undamaged structures may vary considerably from structure to structure, therefore, it is necessary to perform tests on parts that are known to be undamaged in order to estimate typical percent differences. Once these typical percent differences are found, however, this technique eliminates the need to take baseline data to detect damage.

4.2 Detailed description of power spectral density technique

The second technique developed involves the calculation of the power spectral density (PSD) for each signal acquired. The PSD is calculated using Welch's averaged modified periodogram method of spectral estimation with no overlapping samples. Once the PSD has been calculated for the first A_0 mode arrival for each of the equal length paths, the area under each curve is determined using the trapezoidal rule, giving the average power of the signal. The mean value of the average power for all equal length paths is then calculated. The mean power value is then compared to each individual path by calculating a percent difference for each path, as defined by (7). The percent difference is multiplied by negative one so that signals with a greater average power will show a positive percent difference and signals with a lower average power will show a negative percent difference.

$$percent \quad difference(i) = \frac{mean \quad power - power(i)}{mean \quad power} * (-1) \tag{7}$$

Through this technique, any signal that has a statistically increased or decreased average power can be identified and differentiated. This allows for recognition of both attenuated and amplified signals. Similar to the cross correlation method, a threshold on percent difference must also be set for the PSD technique. Again, as long as typical percent differences for undamaged parts can be estimated, no pre-recorded baseline data is necessary for damage detection.

4.3 Detailed description of Proper Orthogonal Decomposition technique

The final data processing technique developed is based on the concept of Proper Orthogonal Decomposition (POD). The method works to compare the most dominant mode of each equal length path signal to identify damage. Changes in the dominant component of each signal are used to determine how well each signal is correlated with the other signals. First, a correlation matrix is made by sampling one data point for each equal length path at a certain point in time. The correlation matrix is defined in (8), where $\mathbf{p}$ is the vector containing one data point from each equal length path at a given point in time.

$$C_{ij} = \mathbf{p}_i \mathbf{p}_j \tag{8}$$

The correlation matrix is built for each time step during the arrival of the first A_0 mode and then time averaged based on the number of time steps used, n, according to (9).

$$C_{avg} = \sum_{i=1}^{n} \frac{C(i)}{n} \tag{9}$$

In order to determine the dominant modes that exist in the time averaged matrix, its eigenvalues and eigenvectors are calculated. In an ideal case where all of the signals from equal length paths are nearly identical, only one orthogonal mode would be necessary to represent all of the signals, hence, the first eigenvalue would far outweigh all the other eigenvalues. One way to detect damage is to calculate the ratio of the second eigenvalue over the first eigenvalue. If this ratio is above some threshold, then it can be concluded that there are two or more orthogonal modes needed to represent the signals, thus the signals are not well correlated. To identify which path is damaged, the index of the highest entry of the second eigenvalue is found. This index corresponds to the path for which the second orthogonal mode is required to represent its signal, hence it represent the path that does not correlate well with the others. Damage is often not significant enough to cause more than one orthogonal mode to be required to represent the signals. In this case, damage can be detected by analyzing the entries of the first eigenvector, which signify how well the first orthogonal mode represents each path signal. Damaged paths are detected by performing a percent difference calculation as shown in (10), by calculating the mean of the eigenvector entries and comparing each individual entry to the mean.

$$percent \quad difference(i) = \frac{mean \quad entry - entry(i)}{mean \quad entry} \tag{10}$$

Once the percent differences are calculated for each path, the highest percent difference value is compared to a threshold. If the value is higher than the threshold, it is removed from the data set, and the process is continued until the highest percent difference is below the threshold, similar to the cross correlation method. All of the paths that were removed are declared damaged. Like the previous techniques, a threshold must be set on the percent difference, but with knowledge of typical undamaged structures, damage can be detected without pre-recorded baseline data.

5. EXPERIMENTAL TESTING AND RESULTS

Several sets of data were acquired for undamaged plates to determine test-to-test and path-to-path signal variability. After these undamaged sets of data were acquired, reversible damage in the form of industrial putty was applied to the plates to add mass and simulate damage. The putty provided a removable damage case that could be moved to any

location on the plate in order to establish the sensitivity of each path to damage and to test the signal processing algorithms described in the previous section of the paper. In order to determine the sensitivity of the technique to a real-world type of damage, corrosion was induced in two of the plates. Several sizes and shapes of corrosion were induced to simulate variations found in natural corrosion. Lastly, a cut was slowly introduced into the third plate using a Dremel tool, and data was recorded at several discrete depth intervals until the back side of the plate was breached. The cut was created to simulate a second type of real-world damage.

5.1 Undamaged plate

The first few sets of data recorded on all of the plates used in this study were taken on undamaged plates. Typical undamaged time histories for both the square and circular PZT pattern can be seen in Figure 5.

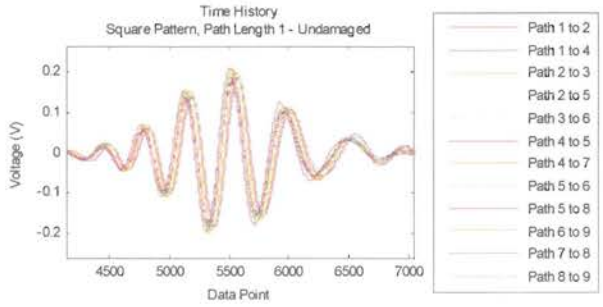

(b) Square Pattern: Path Length 1

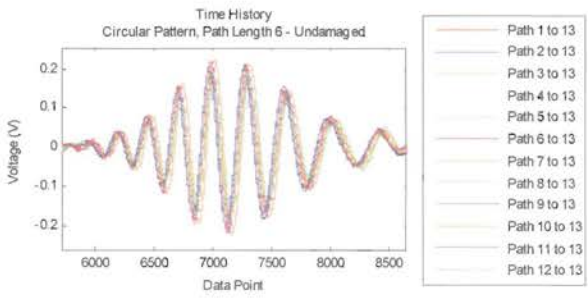

(a) Circular Pattern: Path Length 6

Figure 5: Time history plots for typical undamaged square pattern plate

The undamaged time histories were used to determine the typical signal variation of each path length for the square and circular pattern in order to help establish the sensitivity of the proposed instantaneous baseline technique. All of the data sets taken from undamaged cases were analyzed using the cross correlation, PSD, and POD methods to determine usual percent differences when no damage is present. The threshold on percent difference for each technique must be set significantly higher than any of the observed percent differences on the undamaged plates. Typical values of percent differences and POD ratio for all three analysis techniques are shown in Tables 8 and 9 for the square and circular configuration, respectively. Based on changes in the percent differences observed for a variety of damaged cases, it can be concluded that in the plate structures explored, increases of 10%-20% above the normal undamaged percentages indicate paths of questionable condition, and increases above 20% indicate damaged paths.

Table 8: Typical percent differences for square pattern plate

	Data Analysis Technique			
Path Length	Cross Correlation	PSD	POD	POD Ratio
1	20%	20%	20%	0.13
2	26%	13%	15%	0.13
3	26%	30%	20%	0.09

Table 9: Typical percent differences for circular pattern plate

	Data Analysis Technique			
Path Length	Cross Correlation	PSD	POD	POD Ratio
1	25%	45%	60%	0.30
2	25%	40%	120%	0.40
3	20%	40%	180%	0.55
4	30%	40%	65%	0.25
5	15%	35%	50%	0.20
6	15%	25%	20%	0.13

5.2 Removable putty damage

The first damage case investigated involved placing removable putty in various locations on the aluminum plates. Figure 6a shows a photograph of the first square pattern aluminum plate with a large piece of removable putty placed between patches 2 and 3. The time domain plot of the data recorded during this test is shown in Figure 6b. From the time domain

plot, it is clear that the damaged path is severely attenuated. Visual based detection works well in this case; however, the signal may not always be distorted to this extent. Additionally, the visual method relies on human interaction to detect damage. For these reasons, the three data analysis techniques developed in this study were implemented.

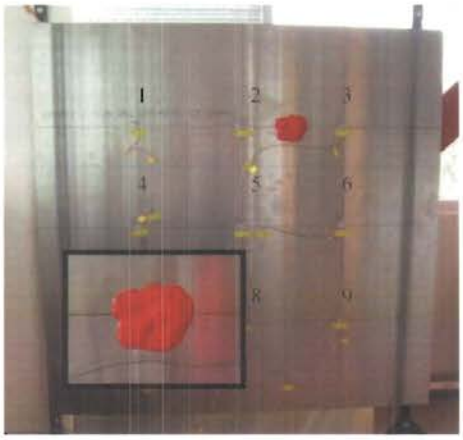

(a) Photograph of removable putty damage

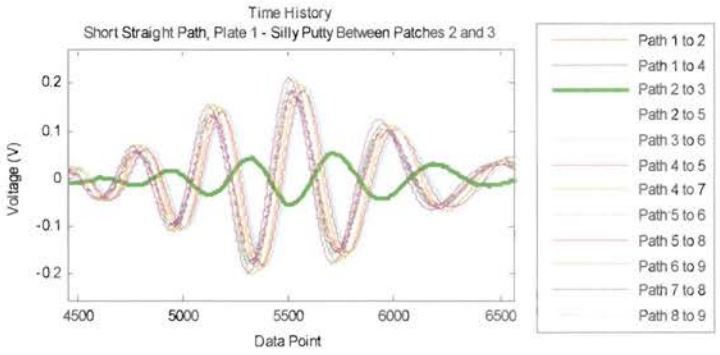

(b) Time history for short straight path lengths

Figure 6: Photograph of and time history for square pattern with putty placed between patches 2 and 3

Upon analyzing the data using the cross correlation, PSD, and POD methods, the damaged path was easily detected. For an example of the output graphs for each technique, Figure 7a and 7b show the graphs of the modified correlation coefficients calculated for the cross correlation method. From these figures, it is clear that path 2-3 is identified as an outlier. A percent difference of 91.78% was found after removing path 2-3 from the data set, which is well above the threshold of 20% above the normal percent difference reported in Table 8. Figure 7c shows the power spectral density estimates calculated for the PSD method. Again, path 2-3 can be easily identified as an outlier in the data set. A percent difference of -90.86% was found between the average area under each PSD curve and the area under the curve for path 2-3, which is much higher than the threshold for this path length. Lastly, the POD method, for which there are no meaningful graphs to present, calculated a 131.10% difference in the entries of the first eigenvector for path 2-3. Again, this percent difference is much higher than the threshold. Based on these results, the three analysis techniques were found to confidently detect large putty damage for the square pattern.

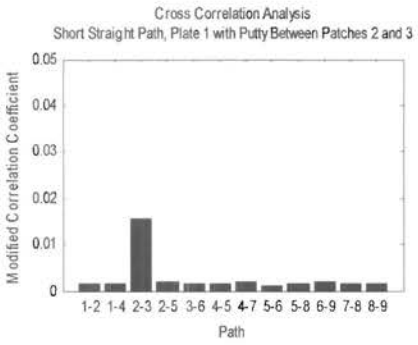

(a) Cross correlation analysis before removing path 2-3

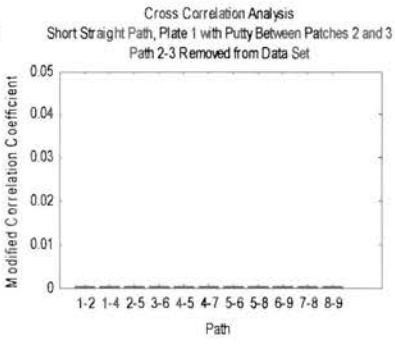

(b) Cross correlation analysis after removing path 2-3

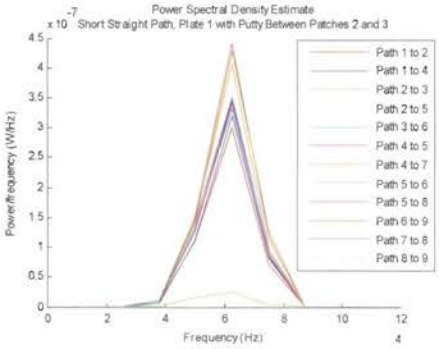

(c) Power Spectral Density plot

Figure 7: Analysis graphs for square pattern plate with putty placed between patches 2 and 3

Removable putty damage tests were also run for the circular pattern plate, and similar results were found. With a large piece of putty placed between patches 11 and 13, several paths that crossed near the putty were indicated as damaged for all three data analysis techniques. The fact that several paths were indicated as damaged suggests that the location of the

damage may also be found using based on the intersection of the damaged paths. This concept of locating damage will be further explored in the following section of the paper when analyzing the various corrosion damages induced in the plates.

5.3 Corrosion damage

Once it was shown that the cross correlation, PSD, and POD methods were capable of detecting removable putty damage, permanent damage in the form of corrosion was induced onto two of the plates to better represent real-world damage. Several shapes and sizes of corrosion were induced and tested. Figure 8 shows photographs of each damage site as well as a graphical illustration of the damage sites and the paths successfully identified with each technique.

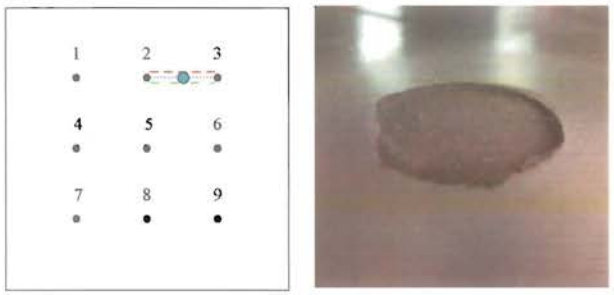

(a) Small corrosion path 2-3 on square plate

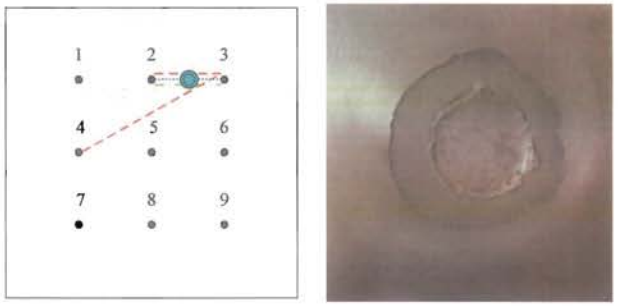

(b) Concentric circle corrosion path 2-3 on square plate

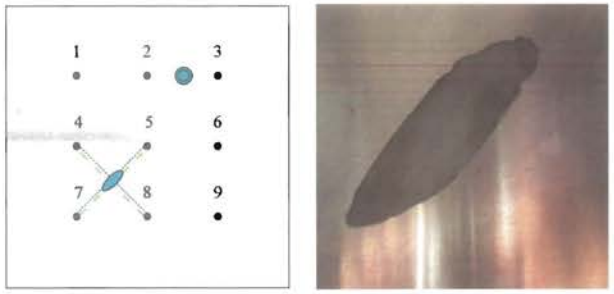

(c) Oblong corrosion path 5-7, 4-8 on square plate

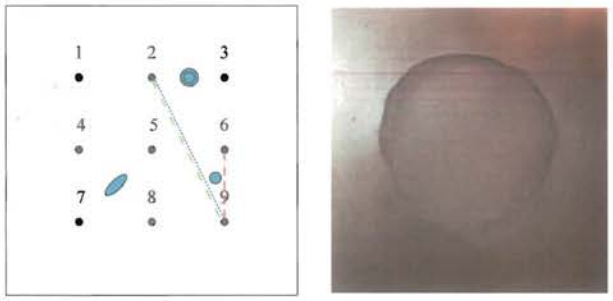

(d) Off-path circle corrosion path 6-9 on square plate

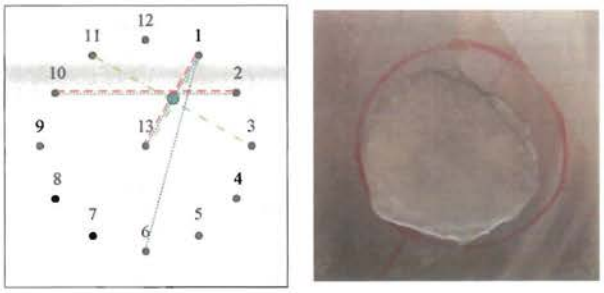

(e) Small corrosion path 1-13 on circular plate

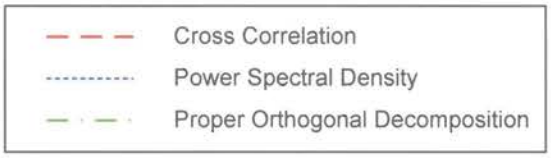

Figure 8: Various corrosion cases studied along with paths identified as damaged for each analysis technique

Figure 8a shows a small corrosion site induced between patches 2 and 3 on the square pattern plate measuring 1.04 in (26.42 mm) in diameter. This was the first corrosion type tested, and the corrosion was induced in nine discrete depth intervals from 0.004 in (0.102 mm) to 0.033 in (0.838 mm) to help determine the sensitivity of each data analysis technique versus the depth of corrosion. A concentric circle of less severe corrosion, shown in Figure 8b, was later added around the initial small circle. The concentric circle corrosion was induced to simulate the variations found in

real-world corrosion damage and had a final diameter and depth of 1.84 in (46.74 mm) and 0.018 in (0.46 mm), respectively. An elliptical corrosion site, seen in Figure 8c, was created next to explore the effects of non-circular corrosion. The dimensions of the elliptical corrosion were 3.83 in (97.28 mm) long by 1.12 in (28.45 mm) wide with a depth of 0.023 in (0.58 mm). The final corrosion damage induced in the square pattern plate was placed in an area not directly crossed by one of the actuator-sensor paths. By locating damage out of the direct paths, the sensitivity of the signals to nearby damage can be determined. The corrosion induced to monitor off-path sensitivity was a circle with a 1.24 in (31.50 mm) diameter and a 0.02 in (0.51 mm) depth. Corrosion was also induced in the circular pattern plate between patches 1 and 13 to compare the ability of the square and circular patterns to detect damage. The corrosion measured 1.75 in (44.45 mm) in diameter and 0.02 in (0.51 mm) deep.

From the resulting damage paths shown in Figure 8 for all of the corrosion types, it is clear that a combination of all three data analysis techniques results in the successful identification of damage in each case. With the exception of the oblong corrosion shown in Figure 8c, each analysis technique was able to detect every corrosion site induced in the plates. Additionally, a combination of all three analysis methods yields the ability to locate damage as well.

Based on the nine depth intervals tested for the first circular corrosion between patches 2 and 3 on the square pattern plate, it was determined that the cross correlation method was capable of detecting damage at depths above approximately 0.029 in (0.737 mm). The PSD technique detected damage for all depths above 0.016 in (0.406 mm) except for a depth of 0.029 in (0.737 mm). Upon analyzing this time domain data for each increasing depth, it was found that initially the corrosion causes the amplitude of the damaged path to increase, which was unexpected, however, signal amplification due to corrosion has been found in other research.[5] Once the depth increased beyond 0.021 in (0.533 mm), the time history signal began to attenuate. At a depth of 0.029 in (0.737 mm), where the PSD method was unable to detect the damage, the amplitude of the damaged signal was approximately equal to the amplitude of the undamaged signals. The PSD technique analyzes the energy in each signal, hence the inability of the PSD technique to identify damage when the signal amplitude is approximately equal to the undamaged signal. It is suspected that the inability of the PSD method to detect damage will only occur over a small range of depths. Lastly, the POD technique, like the cross correlation method, was found to detect damage at depths above 0.029 in (0.737 mm).

Based on the results shown in Figures 8b-8d, it can be concluded that corrosion with non-uniform depth, oblong corrosion, and corrosion not directly placed in the path of two PZT patches can all be detected using a combination of detection methods. Percent differences of the damaged paths shown in these figures vary from 50% to 120%. This variation is related to the size, shape, depth, and location of the corrosion relative to the path. Preliminary analysis has been conducted to investigate the effects of these variables on the ability of each technique to detect damage; however, further tests must be run to confirm these results.

The corrosion induced on the circular pattern plate, shown in Figure 8e, was used to compare the sensitivity of the circular PZT pattern versus the square pattern in detecting damage. Although the square pattern proved capable of detecting all damage types induced in the plate, a comparison of the damaged paths identified for both the square and circular configuration shows that the circular pattern is more capable of determining the exact location of damage. This is mostly due to the fact that there is much better part coverage for the circular pattern (see Figure 4b) than the square pattern (see Figure 3b), so more than just one or two paths are identified as damaged. The intersection of all the damaged paths can be used to identify the location of damage. The drawback to the circular configuration is that it requires more PZT patches and more data processing because there are twice as many paths to analyze. Depending on the structure to be analyzed, these results can be used to select an appropriate sensor pattern based on the desired part coverage and data processing requirements.

5.4 Cut damage

A third aluminum plate was instrumented with a square PZT pattern and a cut was slowly induced between patches 1 and 2. The depth of the cut, which can be seen in Figure 9, was increased at discrete intervals until the back side of the plate was breached. After the final cut was made, the void in the plate was approximately 0.04 in (1.02 mm) wide and 0.8 in (20.32 mm) long.

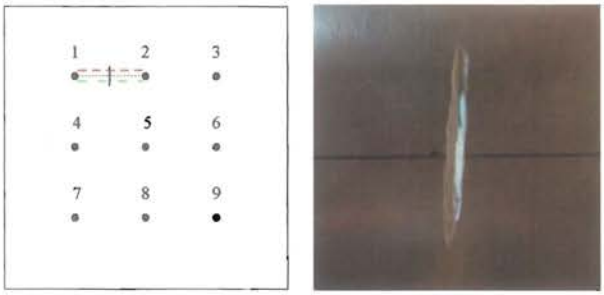

Figure 9: Cut damage and damaged paths for each analysis technique

Upon analyzing the data, all three analysis methods were capable of detecting the final cut that breached the plate. This result is shown graphically in Figure 9 for which the legend is the same as seen in Figure 8. Although the three techniques were able to detect the cut when it was completely through the plate, none of the methods were able to detect the damage for the first five depth levels. The cross correlation and POD methods were able to detect the damage for the sixth depth when the cut was almost through the plate, and the PSD technique could only detect the cut when it was through the plate.

6. CONCLUSIONS

The instantaneous baseline technique developed in this study has been successful in detecting damage in the three aluminum plates studied. With the combination of the cross correlation, power spectral density, and proper orthogonal decomposition approaches, all damaged paths were identified for the putty, corrosion, and cut damage. Overall it seems as though the circular PZT configuration offers better part coverage and better ability to find the exact location of damage, however it requires more PZT patches. There are, however, some limitations that have been discovered while performing this research and data analysis. The statistical nature with which the instantaneous baseline is developed puts significant limitations on the number of damaged paths that can exist in a part and still allow the damage to be identified. If the ratio of damaged paths to undamaged paths is too high, the techniques will be unable to create an effective baseline. Another limitation of the technique is that real-world structures will contain complexities such as fasteners and geometrical changes, which will cause the undamaged paths to show more variation resulting in a lower sensitivity to damage because the percent difference threshold must be increased to accommodate for these variations. Future work may involve modeling the interaction between Lamb waves and different types of damage. Additionally, further experiments must be run on parts with more complex geometry including fasteners and stiffeners.

7. REFERENCES

1. Simmers Jr., G.E., Sodano, H.A., Park, G., Inman, D.J., "Detection of corrosion using piezoelectric impedance-based structural health monitoring," AIAA Journal, Vol. 44, No. 11, pp. 2800-2803, 2006.
2. Grisso, B.L., Inman, D.J., "Impedance-based structural health monitoring of thermal protection systems," Proceedings of SPIE - The International Society for Optical Engineering, Vol. 6176, Nondestructive Evaluation and Health Monitoring of Aerospace Materials, Composites, and Civil Infrastructure V, p 61760M, 2006.
3. Kessler, S.S., Spearing, S.M., and Soutis, C., "Damage detection in composite materials using Lamb wave methods," Smart Materials and Structures, Vol. 11, No. 2, pp. 269-278, 2002.
4. Sohn, H., Park, G., Wait, J.R., Limback, N.P., and Farrar, C.R., "Wavelet-based signal processing for detecting delamination in composite plates," Smart Materials and Structures, Vol. 13, No. 1, pp. 153-160, 2004.
5. Thomas, D., Welter, J., and Giurgiutiu, V., "Corrosion damage detection with piezoelectric wafer active sensors," Proceedings of SPIE - The International Society for Optical Engineering, Vol. 5394, Health Monitoring and Smart Nondestructive Evaluation of Structural and Biological Systems III, pp. 11-22, 2004.
6. Viktorov, I.A., "Rayleigh and Lamb Waves," Plenum Press, New York, 1967.
7. Park, G., Farrar, C., Rutherford, C., and Robertson, A., "Piezoelectric active sensor self-diagnostics using electrical admittance measurements," ASME Journal of Vibration and Acoustics, Vol. 128, No. 4, pp. 469-476, 2006.
8. Park, G., Farrar, C., Lanza di Scalea, F., and Coccia, S., "Performance assessment and validation of piezoelectric active sensors in structural health monitoring," Smart Materials and Structures, Vol. 15, No. 6, pp. 1673-1683, 2006.